LANGMUIR

Article

pubs.acs.org/Langmuir

Self-Assembled Hierarchical Arrays for Colored Retroreflective Coatings

Kuan-Yi Tsao,[†] Hui-Ping Tsai,[‡] Kun-Yi Andrew Lin,[§] Yi-Xuan He,[†] and Hongta Yang*[,†]

[†]Department of Chemical Engineering, [‡]Department of Civil Engineering, and [§]Department of Environmental Engineering, National Chung Hsing University, 145 Xingda Road, Taichung City 40227, Taiwan

Supporting Information

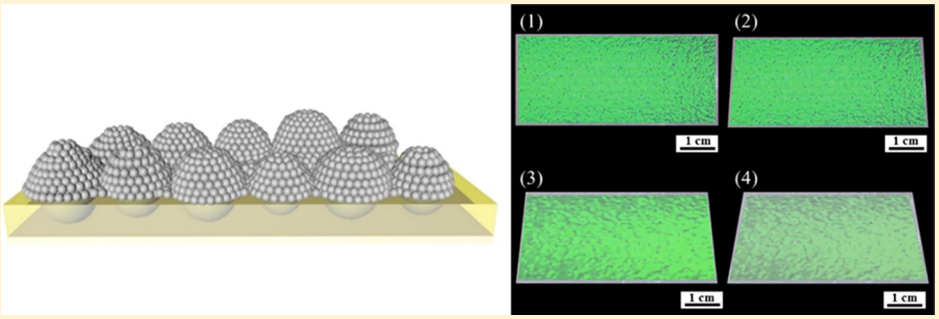

ABSTRACT: This study reports a self-assembly technology for fabricating retroreflection coatings with hierarchical nano-/microstructures, which are inspired by the binary periodic structures found in the compound eyes of insects. Silica colloidal crystals of adjustable thicknesses are assembled on encountering glass microbeads using a Langmuir−Blodgett-like approach in a layer-by-layer manner. The as-assembled hierarchical structures exhibit a brilliant color caused by Bragg diffraction from the crystalline lattice of silica colloidal crystals on glass microbeads. The resultant coating is capable of reflecting light in the opposite direction of the incident light. Moreover, the dependence of the silica particle size, the colloidal crystal thickness, and the incident angle on the retroreflective properties are investigated in this study.

INTRODUCTION

Retroreflective materials include an array of transparent retroreflective elements, such as glass microbeads, triangular microprisms, and cube corner microprisms, partially embedded with a reflective undercoating in a binder layer, which in turn binds the embedded elements to a layered material.[1−3] This type of material can reflect light back in a very narrow beam along a vector that is parallel but opposite to the direction of the light source.[4] Unlike for a planar mirror, the incident angle at which the material reflects light in this way is greater than zero. Owing to this unique feature, the retroreflective materials have been widely used to increase the visibility of traffic signs, vehicle operators, and safety clothing.[5−10] In addition, retroreflective materials can enhance detection in measurement systems and operate as reflecting units in optical communication equipment.[9−13] Additional applications such as building coatings for preventing the urban heat island effect have also been reported.[14,15] However, the use of metalized aluminum layer as a reflective undercoating leads to silver coloration, which is undesirable in many applications.[16,17]

To address the aforementioned issues, commercial colorants, such as fluorescent dyes and pigments, are introduced to create colored retroreflective materials. Nevertheless, the application of colorants seriously impedes the interaction between the retroreflective elements and the undercoating layers, resulting in a low color fastness to laundering and poor weathering resistance.[18] In addition, because of weak ultraviolet resistance, most colorants change color and lose intensity over time.[19] Therefore, commercial colored retroreflective materials suffer from color deterioration and color fading over short-term use. Furthermore, the limited choices of colorants and the complicated manufacturing process seriously restrict their development.[20] By contrast, applying a color plastic layer on the retroreflective materials above the partially exposed surfaces of the retroreflective elements provides a much simpler and inexpensive alternative to creating colored retroreflective materials. Nevertheless, the plastic layer impedes the inherent retroreflective properties of the colored retroreflective materials.[21]

Natural biological systems have developed many sub-microscale architectures to create advanced functionalities through decades of evolution.[22,23] For instance, the compound eyes of many insects are comprised of thousands of microscale ommatidia that increase the field of view and the capability of fast tracking of moving objects.[24] The ommatidia are covered by highly ordered sub-microscale protuberances, which potentially improves visual efficiency through increased photon capture for a given stimulus.[25] The periodic hierarchical arrays exhibit a

Received: September 8, 2016
Revised: October 11, 2016
Published: November 5, 2016

DOI: 10.1021/acs.langmuir.6b03329
Langmuir 2016, 32, 12869−12875

unique optical diffraction caused by Bragg diffraction at various viewing angles.[26]

To mimic the hierarchically structured insect compound eyes, this study aims to create photonic crystals on the surfaces of microscale retroreflective arrays to fabricate colored retroreflective materials. Compared with complex lithography-based top−down fabrication technologies, self-assembly of monodisperse colloidal particles provides a simpler approach for developing photonic crystals.[27] Recently, many bottom−up self-assembly methodologies, including dip-coating, spin-coating, capillary force-induced self-assembly, and electrical field-induced self-assembly, have been employed to build hierarchical structures.[28−31] Unfortunately, the resultant particle arrays are randomly arranged or the size of the prepared hierarchical structures does not match those of the insect compound eyes. These drawbacks significantly affect the uniformity of the structured colored retroreflective materials. By coating metals on the hemispherical surface of microparticles, retroreflective Janus microparticles have been developed for highly reflective coatings, which respond to polychromatic white light sources.[32,33] However, the approaches are limited by low volume and high production cost.[34] Here, we report a scalable Langmuir−Blodgett (LB) technology that can be used for assembling submicrometer-scale silica colloidal crystals on the surfaces of retroreflective elements, mimicking those of natural cornel eyes.

EXPERIMENTAL SECTION

Materials and Substrates. All chemicals were of reagent quality and were used without further purification. The reagents used for silica sphere synthesis, including tetraethyl orthosilicate (TEOS) (98%), ammonium hydroxide (NH_4OH) (28%), and absolute ethanol (99.5%), were purchased from Sigma-Aldrich. Deionized water (18.2 MΩ cm) from a Millipore A-10 water purification system was used. The ethoxylated trimethylolpropane triacrylate monomer (ETPTA, SR 454) and the photoinitiator 2-hydroxy-2-methyl-1-phenyl-1-propanone (Darocur 1173) were provided by Sartomer and BASF, respectively. Commercial retroreflective materials and poly(ethylene terephthalate) (PET) sheets with a monolayer of glass microspheres partially embedded on the surface were offered by Maystar Reflex Technology. In the commercial fabrication process, PET films (0.075 mm thick, Wisegate Technology) and silica glass microspheres (30−70 μm in diameter, Golden Fountain) were rinsed with water and then dried at room temperature. The cleaned glass microspheres were deposited on the PET film that was coated with a layer of a release agent, and pressed at 190 °C with a pressure that would embed the microspheres into the release agent layer to create glass microsphere-embedded PET sheets. The exposed size and height of the spherical caps of the embedded glass microspheres ranged from 10 to 50 μm (Figure S1). The interparticle distance of the glass microspheres was approximately 5 μm on average, whereas some 10 micrometer-scale vacancies were present. The PET sheets were semifinished products used for fabricating commercial retroreflective materials. An approximately 50 nm-thick aluminum layer was deposited onto the PET sheets by sputtering, followed by casting with a hot melt adhesive, and covering with polyurethane (PU) films. After drying, commercial retroreflective materials including a monolayer of glass microspheres partially embedded with a reflective aluminum undercoating in a binder layer could be peeled off from the release agent layer.

Preparation of Colloidal Suspensions. Monodispersed silica spheres of 300, 250, and 210 nm diameters were synthesized using the Stöber method.[35] In this study, TEOS was rapidly added to a mixture of NH_4OH, absolute ethanol, and deionized water and hydrolyzed to form silica spheres at ambient temperature over 24 h. The as-synthesized Stöber silica spheres were purified using absolute ethanol by several centrifugation/redispersion cycles to completely remove impurities and unreacted chemicals, followed by redispersing in nonvolatile ETPTA monomers with 1 vol % Darocur 1173 as the photoinitiator using a Thermolyne vortex mixer. After filtering through a 5 μm syringe filter (Whatman), the transparent silica colloidal suspensions were stored in an open vial in the dark for 12 h to evaporate the residual ethanol.

Fabrication of Hierarchical Arrays. The procedure for fabrication of hierarchical arrays is displayed in Figure 1. Using a clamp attached to a syringe pump, a cleaned PET sheet with partially embedded glass microspheres was vertically immersed in a dish containing deionized water. The as-prepared colloidal suspension was added to the deionized water surface. Owing to the high surface tension of water, the floating monomer-covered silica spheres rapidly dispersed and self-assembled into close-packed colloidal crystals because of the capillary action between the neighboring silica spheres at the air/water interface. The crystalline quality of the colloidal arrays was further improved by gently tapping the dish to procure the merging of crystal domains. The PET sheet was then withdrawn vertically at a constant rate of ∼5 cm/min controlled by a syringe pump (KD Scientific 780-230). Meanwhile, the floating two-dimensional silica colloidal crystals were deposited on the contoured surfaces of the hydrophilic glass microspheres, which were partially embedded on the surface of the PET sheet. After drying, the PET sheet was reimmersed in deionized water, and another monolayer of colloidal crystals was subsequently transferred onto the substrate. By repeating the fabrication process, the hierarchical arrays consisting of three-dimensional (3D) colloidal crystals with an adjustable layer number were prepared. The sample was finally transferred to a pulsed UV curing system to photopolymerize the ETPTA monomers, to prevent the monomers from flowing and filling the empty space between the silica spheres by gravity and capillary action.

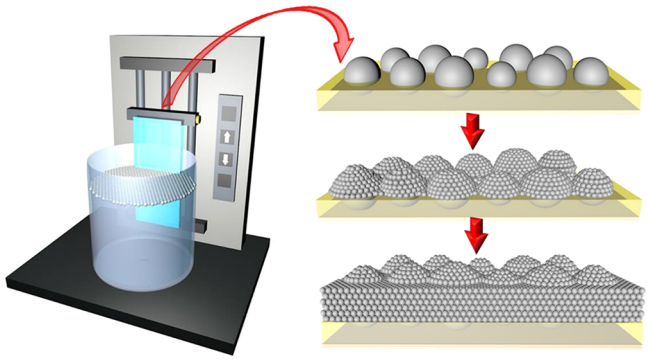

Figure 1. Schematic illustration of the experimental procedure for the fabrication of colored retroreflective coatings with hierarchical arrays.

Characterization. Scanning electron microscopy (SEM) was performed using a JEOL 6335F FEG scanning electron microscope. A thin layer of platinum was sputtered onto the samples before imaging. Photographs of the samples were acquired using a Nikon Coolpix L810 digital compact camera. The high-resolution fiber-optic UV−visible−near-infrared (IR) spectrometer HR4000 from Ocean Optics was used in characterizing the optical retroreflection spectra. The cone angle of collection was less than 1°, which is within the range of the most commonly used traffic control devices (0.1° to 1°). The spectra were recorded using the SpectraSuite spectroscopy software from Ocean Optics over a wavelength range of 300−800 nm.

RESULTS AND DISCUSSION

Figure 2a shows the images of assembled hierarchical arrays consisting of 25-layered 250 nm silica colloidal crystals illuminated with white light. The coating exhibits a uniform green color at normal incidence and normal viewing (Figure 2a1). Compared with the commercial retroreflective coatings shown in Figure S2, the brilliant color is the result of Bragg diffraction of incident visible light from the crystalline lattice. Importantly, a change in color is not observed as the incident angle and the viewing angle are increased simultaneously from 0° (normal incidence) to 30° (Figure 2a). In addition, it is found

DOI: 10.1021/acs.langmuir.6b03329
Langmuir 2016, 32, 12869−12875

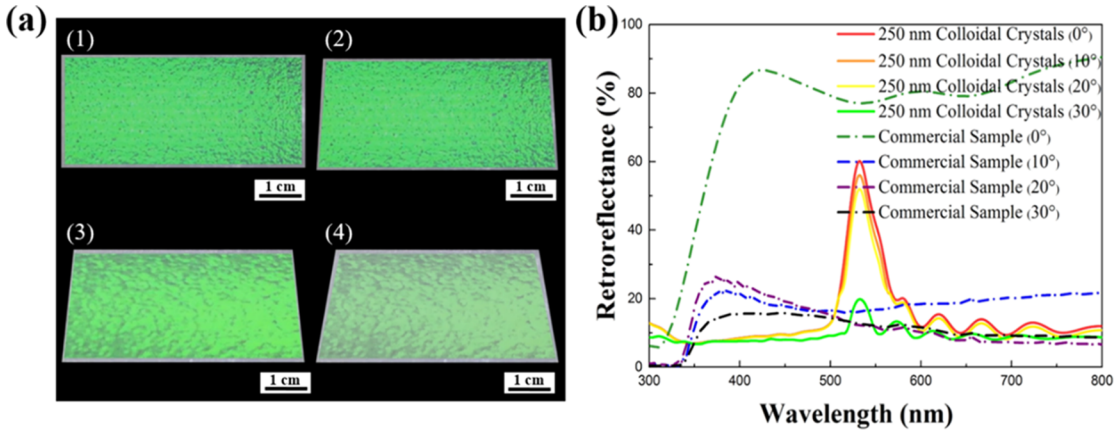

Figure 2. (a) Photographs of the assembled retroreflective coatings consisting of 250 nm silica colloidal crystals (~25 layers thick) taken from different angles: (1) 0°, (2) 10°, (3) 20°, and (4) 30°. (b) Optical retroreflection spectra obtained from the as-fabricated sample and a commercial sample at various incident angles.

that the color brightness decreased with the increase in the viewing angle. There is a noticeable decrease in the brightness as the viewing angle reaches 30°.

To further evaluate the optical properties of the as-fabricated coating, a UV−vis−NIR Ocean Optics spectrometer was used to measure the retroreflectance at various incident angles. Here, the retroreflectance of a coating is defined as the ratio between the light leaving the surface in the opposite direction to the incident light and the incident light encountering the surface. The retroreflection spectra obtained from the assembled retroreflective coatings consisting of 25-layered 250 nm silica colloidal crystals are presented in Figure 2b, where the measured retroreflectance of the commercial retroreflective coatings are shown as references. The commercial retroreflective coating exhibits a retroreflectance of approximately 80% in the range of wavelengths within the visible light spectrum at normal incidence and normal viewing. Additionally, the retroreflectance significantly decreases with the increase in the incident angle. The results can be described as a combination of Snell's law and Fresnel's formula.[36] When light enters and leaves the glass beads, the light is bent by refraction and thereby some light loss occurs at the surface. Besides that, the coating consisting of spherical glass beads with a broad size distribution (Figure S3) suffers heavily from high divergence through spherical aberration, referring to the allowance of small entrance angles.[37] The reflection loss and the spherical aberration mentioned above restrain the retroreflection greatly with the increase in the incident angle, leading to low angularity.[38]

Compared with the retroreflection spectrum of the commercial sample, the green lines display the measured retroreflection peaks of the assembled hierarchical arrays at various incident angles located at 536 nm. The distinctive peaks are caused by Bragg diffraction of the incident light from the 3D 250 nm silica colloidal crystals coated on the micrometer-scale glass beads (Figure 3). The high flexibility of the thin water layer during the particle transfer process and the strong capillary action between the silica spheres contribute to the hexagonally ordered silica colloidal crystals on the contoured surfaces of glass beads. The capillary forces during the assembly process cause cracking of the deposited colloidal crystals.[39] Although cracks are observed in most samples, they do not significantly affect the optical properties of the coatings. All spectra display distinct Bragg diffraction peaks with well-defined Fabry−Pérot fringes, indicating the high crystalline quality of the self-assembled

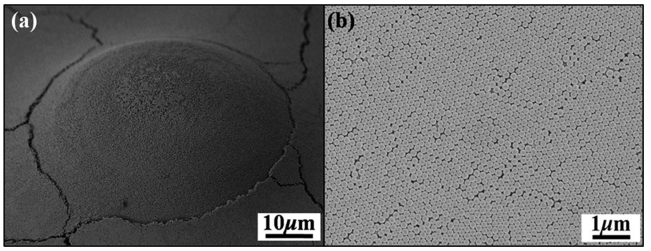

Figure 3. (a) Top-view SEM image of the assembled retroreflective coatings consisting of 250 nm silica colloidal crystals (~25 layers thick). (b) Magnified image of (a).

colloidal crystals. The diffraction peak position can be complemented by theoretical calculation using the Bragg's law[40]

$$\lambda_{peak} = 2n_{eff}d \sin\theta$$

where n_{eff} is the effective refractive index of the medium, d is the interlayer spacing, and sin θ equals 1 at normal incidence. By assuming that the colloidal crystals are closed-packed and the volume fraction of silica is 0.74, the effective refractive index can be estimated by $n_{eff} = n_{silica} \times 0.74 + n_{air} \times 0.26$ where n_{silica} and n_{air} are 1.42 and 1.0, respectively. In addition, the interlayer spacing can be expressed using the formula $d = \sqrt{\frac{2}{3}} \times D$ where D is the particle diameter. The estimated peak position located at 535 nm is in good agreement with the experimental results, confirming the highly crystalline quality of the self-assembled colloidal crystals. More importantly, the intensity of the diffraction peak only slightly decreases with the incident angle from 0° to 20°. This indicates that the effect of spherical aberration can be suppressed by coating with colloidal crystals.

To further comprehend the adjustable retroreflectance, the optical properties of the PET sheets coated with different layer numbers of 250 nm silica colloidal crystals are investigated. The layer numbers of the colloidal crystals are 40, 35, 30, 25, 20, 15, 10, and 5. As shown in Figure 4a,b, the assembled hierarchical arrays consisting of 40-layered 250 nm silica colloidal crystals in the upper-left corner display a retroreflectance of around 85% at 535 nm and a striking green color. In comparison with that, the brightness of the green color decreases as the coating layer number decreases from 40 to 5. The systematic change in the color brightness seen at normal viewing is attributed to the

DOI: 10.1021/acs.langmuir.6b03329
Langmuir 2016, 32, 12869−12875

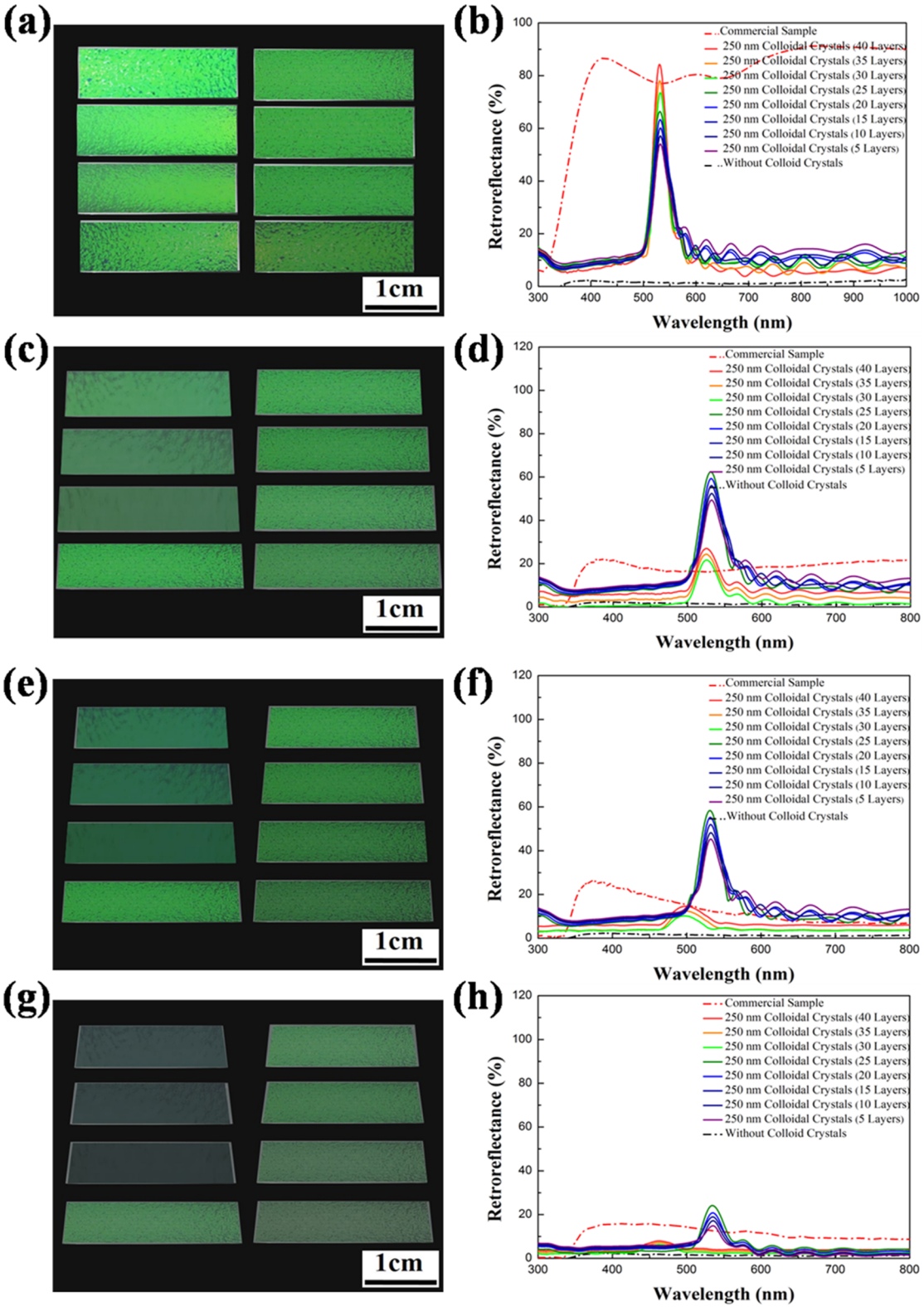

Figure 4. Photographs and optical retroreflection spectra obtained from the assembled retroreflective coatings consisting of 250 nm silica colloidal crystals of varying layers at various incident angles. The layer numbers of the colloidal crystals from the upper left to the lower right are 40, 35, 30, 25, 20, 15, 10, and 5. (a and b) 0°, (c) and (d) 10°, (e) and (f) 20°, and (g) and (h) 30°.

intensity of the Bragg diffraction, which increases approximately linearly with the number of layers.[41]

As revealed in Figure 4c, e, and g, the color brightness and the retroreflectance of the assembled coatings decrease with the increase in the incident angle. It is worthy to mention that the color of the retroreflective coatings consisting of more than 30 layers of colloidal crystals shifts from striking green to dim blue at a larger incident angle. The observed color shift can be explained by the surface morphology of the assembled hierarchical arrays consisting of 40-layered 250 nm silica colloidal crystals in Figure

DOI: 10.1021/acs.langmuir.6b03329
Langmuir 2016, 32, 12869−12875

5. The SEM image displays an ordered close-packed arrangement of silica colloids over a sample area of 10 μm. It is evident that the

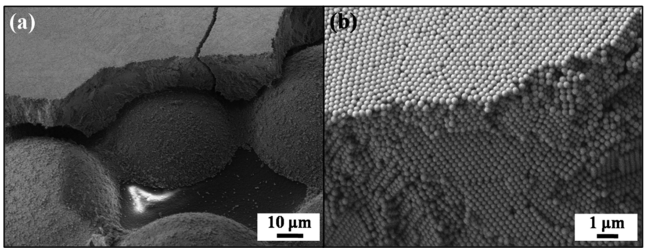

Figure 5. (a) Cross-section SEM image of the assembled retroreflective coatings consisting of 250 nm silica colloidal crystals (~40 layers thick). (b) Magnified image of (a).

stacking of close-packed layers perpendicular to the PET substrate is unaffected by the presence of glass beads on this sample. Owing to the strong capillary actions, the silica colloids can effectively fill the gaps between micrometer-scale glass beads in the deposition procedure, thereby drastically reducing the surface curvature of the glass microspheres after 40 deposition cycles. Therefore, the coatings consisting of more than 30 layers of colloidal crystals function as planar photonic crystals, leading to the color shift and great amplitude reduction of the Bragg diffraction at larger incident angles.

The measured optical retroreflection spectra as illustrated in Figure 4d, f, and h further confirm the visual appearance of the coatings. As the incident angle increases, the spectral retroreflectance curves of the coatings consisting of more than 30 layers of colloidal crystals shift toward lower wavelengths, and the amplitude of each peak decreases. The blue shift of the diffraction peaks can be qualitatively described using Bragg's law, where sin θ equals 0.985, 0.940, and 0.866 as the incident angle reaches 10°, 20°, and 30°, respectively. The calculated diffraction peak positions are located at 527 nm (10°), 502 nm (20°), and 463 nm (30°). It is obvious that the theoretical diffraction peak positions are very close to the measured spectra. Besides, the colors seen at various viewing angles match the spectral retroreflectance found at their respective angles of incidence. The good agreements disclose that the colored retroreflective coating can be achieved by introducing an optimal layer number of colloidal crystals.

To gain a better understanding of the retroreflective properties, close-packed colloidal crystals consisting of 210 nm silica spheres and 300 nm silica spheres are introduced to pattern the hierarchical arrays. Figure 6a displays the photographs of assembled hierarchical arrays consisting of 25-layered 210 nm silica colloidal crystals. The coating exhibits a consistent blue color at various viewing angles. Spectral retroreflectance measurements of the assembled hierarchical arrays are carried out at various incident angles. Figure 6b illustrates the measured retroreflection peaks of the sample at various incident angles located at 450 nm, resulting from the Bragg diffraction of incident light from the 210 nm silica colloidal crystals coated on the glass microspheres. The theoretically estimated position by adopting Bragg's law located at 447 nm matches the experimental results. Similarly, the assembled hierarchical arrays consisting of 25-layered 300 nm silica colloidal crystals display a uniform red color (Figure 7). Both the measured and theoretically estimated Bragg diffraction peaks are located at 639 nm. The results suggest that retroreflective coatings with controllable brilliant color can be fabricated by coating with different-sized silica colloidal crystals.

CONCLUSIONS

In summary, a scalable LB-like technology has been developed to assemble hierarchical arrays consisting of silica colloidal crystals, inspired by the binary structures of the compound eyes of insects. The LB assembly technology enables the spontaneous crystallization of silica spheres with a wide range of sizes into a hexagonal close-packed ordering on encountering curved surfaces. The bioinspired coating exhibits a brilliant color, which can be determined by the size of the silica colloids and the layer number of the colloidal crystals. Because the 3D colloidal crystals are coated uniformly on the surface of glass microspheres, the color change on the as-fabricated coatings is not observed at various viewing angles. Moreover, the spherical aberration effect on retroreflection can be suppressed by coating with colloidal crystals, resulting in a higher angularity. The assembled biomimetic hierarchical arrays with unprecedented optical properties are promising for a wide spectrum of important technological applications in the field of traffic signs, safety clothing, and free-space optical communication networks.

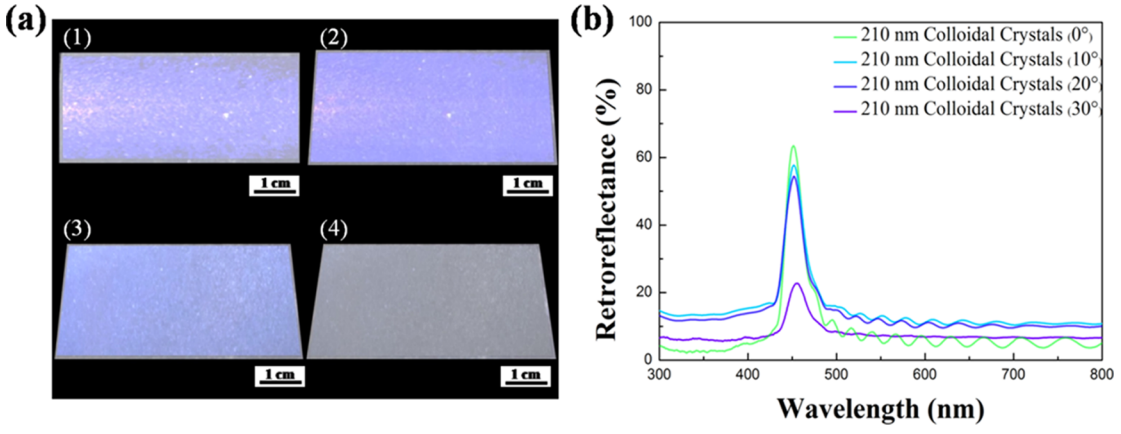

Figure 6. (a) Photographs of the assembled retroreflective coatings consisting of 25-layered 210 nm silica colloidal crystals taken from different angles. (b) Optical retroreflection spectra obtained from the as-fabricated sample and a commercial sample at various incident angles.

DOI: 10.1021/acs.langmuir.6b03329
Langmuir 2016, 32, 12869−12875

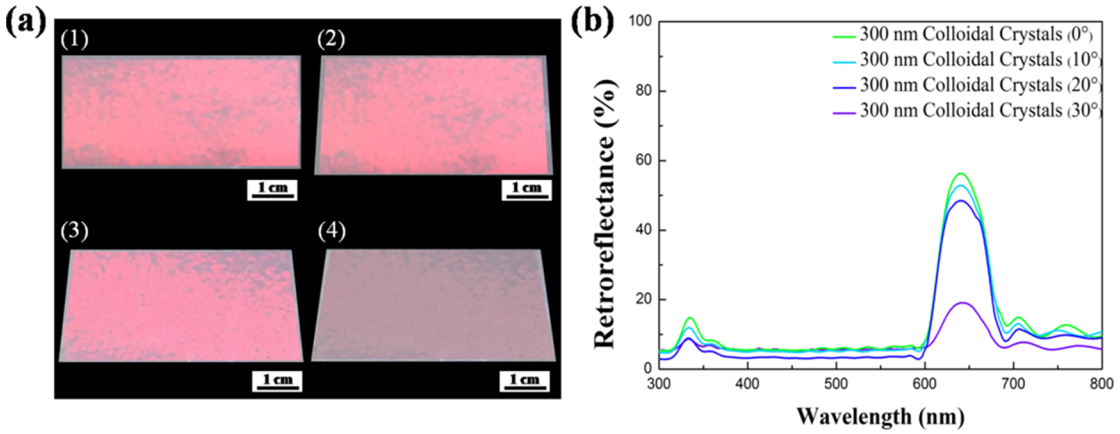

Figure 7. (a) Photographs of the assembled retroreflective coatings consisting of 25-layered 300 nm silica colloidal crystals taken from different angles. (b) Optical retroreflection spectra obtained from the as-fabricated sample and a commercial sample at various incident angles.

■ ASSOCIATED CONTENT

Supporting Information

The Supporting Information is available free of charge on the ACS Publications website at DOI: 10.1021/acs.langmuir.6b03329.

SEM images of a PET sheet with a monolayer of glass microspheres partially embedded on the surface, photographs of a commercial sample taken from different angles, and top-view SEM image of a commercial sample (PDF)

■ AUTHOR INFORMATION

Corresponding Author

*E-mail: hyang@dragon.nchu.edu.tw.

ORCID

Kun-Yi Andrew Lin: 0000-0003-1058-3097

Notes

The authors declare no competing financial interest.

■ ACKNOWLEDGMENTS

The authors acknowledge the support of the Ministry of Science and Technology (Grant MOST 104-2221-E-005-086 and MOST 103-2622-E-005-017-CC3) for this research.

■ REFERENCES

(1) Koppes, R. D.; Brannan, A. K. Colorized retroreflective material and method. US Patent 9248470, 2016.

(2) Karl, B. W. Retroreflective microspheres having a dielectric mirror on a portion of their surface and retroreflective constructions containing such microspheres. US Patent 3700305, 1972.

(3) Lloyd, J. The retroreflective equipment manufacturers association, Lancashire, UK, 2010. http://www.rema.org.uk/.

(4) Wild, N. R.; Leavy, P. M., Jr. Optical detection system. US Patent 6603134, 2003.

(5) Nepal, K. P.; Lahtinen, L. Measurement and analysis of pavement marking retroreflectivity. *Transport Eng. Aust.* **2011**, *13*, 49−60.

(6) Fleming, P. R.; Dahlin, T. J.; Kusilek, T. V.; Smithson, R. L. High contrast retroreflective sheeting and license plates. US Patent 9145098, 2015.

(7) Wood, J. M.; Tyrrell, R. A.; Marszalek, R.; Lacherez, P.; Carberry, T. Bicyclists overestimate their own night-time conspicuity and underestimate the benefits of retroreflective markers on the moveable joints. *Accid. Anal. Prev.* **2013**, *55*, 48−53.

(8) Wood, J. M.; Marszalek, R.; Lacherez, P.; Tyrrell, R. A. Configuring retroreflective markings to enhance the night-time conspicuity of road workers. *Accid. Anal. Prev.* **2014**, *70*, 209−214.

(9) Burgess, G.; Shortis, M. R.; Scott, P. Photographic assessment of retroreflective film properties. *ISPRS Journal of Photogrammetry and Remote Sensing* **2011**, *66*, 743−750.

(10) Zhao, D.; Zhou, H.; Liu, J.; Zhang, B.; Luo, Q. High-precision velocity measuring system for projectiles based on retroreflective laser screen. *Optik* **2013**, *124*, 544−548.

(11) Nakajima, T.; Yokoyama, M.; Muramoto, A.; Orensteen, B. D. Retroreflective sheeting and license plate with reduced retroreflectivity at high entrance angles. US Patent 9110235, 2015.

(12) Goetz, P. G.; Rabinovich, W. S.; Mahon, R.; Murphy, J. L.; Ferraro, M. S.; Suite, M. R.; Smith, W. R.; Burris, H. R.; Moore, C. I.; Schultz, W. W.; Freeman, W. T.; Frawley, S. J.; Mathieu, B. M.; Hacker, K.; Reese, S. Modulating retro-reflector lasercom systems for small unmanned vehicles. *IEEE J. Sel. Area. Comm.* **2012**, *30*, 986−992.

(13) Hyuk-Choon, K.; Won, E.; Bae, T.; Son, J.; Park, D.. Method and apparatus for optical communication using a retro-reflector. US Patent 9118420, 2015.

(14) Yuan, J.; Farnham, C.; Emura, K. Development of a retro-reflective material as building coating and evaluation on albedo of urban canyons and building heat loads. *Energ. Build.* **2015**, *103*, 107−117.

(15) Yuan, J.; Emura, K.; Farnham, C. Geometrical-optics analysis of reflective glass beads applied to building coatings. *Sol. Energy* **2015**, *122*, 997−1010.

(16) Rossi, F.; Castellani, B.; Presciutti, A.; Morini, E.; Filipponi, M.; Nicolini, A.; Santamouris, M. Retroreflective façades for urban heat island mitigation: Experimental investigation and energy evaluations. *Appl. Energy* **2015**, *145*, 8−20.

(17) Rowland, W. P. Colored retroreflective sheeting and method of making same. US Patent 5229882, 1993.

(18) Huang, N.; Klundt, S. M.; Li, H.; Lucas, L. L.; Ray, B. R.; Wu, R. Exposed lens retroreflective article. US Patent 9234990, 2016.

(19) Wu, C. M. Process for reflective products. US Patent 9155346, 2015.

(20) Parisi, A.; Bartoli, C. Process for manufacturing retroreflective printed material. US Patent 7111949, 2006.

(21) Kim, T. I. Advertising sheet using micro-prism retroreflective sheet and method for manufacturing the same. US Patent Application 10/595361, 2004.

(22) Padalkar, S.; Capadona, J. R.; Rowan, S. J.; Weder, C.; Won, Y.-H.; Stanciu, L. A.; Moon, R. J. Natural biopolymers: Novel templates for the synthesis of nanostructures. *Langmuir* **2010**, *26*, 8497−8502.

(23) Zheng, Y.; Bai, H.; Huang, Z.; Tian, X.; Nie, F.-Q.; Zhao, Y.; Zhai, J.; Jiang, L. Directional water collection on wetted spider silk. *Nature* **2010**, *463*, 640−643.

(24) Song, Y. M.; Xie, Y.; Malyarchuk, V.; Xiao, J.; Jung, I.; Choi, K.-J.; Liu, Z.; Park, H.; Lu, C.; Kim, R.-H.; Li, R.; Crozier, K. B.; Huang, Y.; Rogers, J. A. Digital cameras with designs inspired by the arthropod eye. *Nature* **2013**, *497*, 95−99.

DOI: 10.1021/acs.langmuir.6b03329
Langmuir 2016, 32, 12869−12875

(25) Stavenga, D. Colour in the eyes of insects. *J. Comp. Physiol., A* **2002**, *188*, 337−348.
(26) Huang, J.; Wang, X.; Wang, Z. L. Bio-inspired fabrication of antireflection nanostructures by replicating fly eyes. *Nanotechnology* **2007**, *19*, 025602.
(27) Ionov, L. Hydrogel-based actuators: Possibilities and limitations. *Mater. Today* **2014**, *17*, 494−503.
(28) Xiu, Y.; Zhu, L.; Hess, D. W.; Wong, C. P. Biomimetic creation of hierarchical surface structures by combining colloidal self-assembly and Au sputter deposition. *Langmuir* **2006**, *22*, 9676−9681.
(29) Yang, H.; Jiang, P. Scalable fabrication of superhydrophobic hierarchical colloidal arrays. *J. Colloid Interface Sci.* **2010**, *352*, 558−565.
(30) Lee, J.; Seo, J.; Kim, D.; Shin, S.; Lee, S.; Mahata, C.; Lee, H.-S.; Min, B.-W.; Lee, T. Capillary force-induced glue-free printing of Ag nanoparticle arrays for highly sensitive SERS substrates. *ACS Appl. Mater. Interfaces* **2014**, *6*, 9053−9060.
(31) Jin, C.; Olsen, B. C.; Wu, N. L. Y.; Luber, E. J.; Buriak, J. M. Sequential nanopatterned block copolymer self-assembly on surfaces. *Langmuir* **2016**, *32*, 5890−5898.
(32) Han, Y. D.; Kim, H.-S.; Park, Y. M.; Chun, H. J.; Kim, J.-H.; Yoon, H. C. Retroreflective Janus microparticle as a nonspectroscopic optical immunosensing probe. *ACS. Appl. Mater. Interfaces* **2016**, *8*, 10767−10774.
(33) Schultz, P.; Cumby, B.; Heikenfeld, J. Investigation of five types of switchable retroreflector films for enhanced visible and infrared conspicuity applications. *Appl. Opt.* **2012**, *51*, 3744−3754.
(34) Collier, C. M.; Jin, X.; Holzman, J. F.; Cheng, J. Omni-directional characteristics of composite retroreflectors. *J. Opt. A: Pure Appl. Opt.* **2009**, *11*, 085404.
(35) Stöber, W.; Fink, A.; Bohn, E. Controlled growth of monodisperse silica spheres in the micron size range. *J. Colloid Interface Sci.* **1968**, *26*, 62−69.
(36) Biswas, K.; Gangopadhyay, S.; Kim, H.-C.; Miller, R. D. Nanoporous organosilicate films as antireflection coatings. *Thin Solid Films* **2006**, *514*, 350−354.
(37) Lundvall, A.; Nikolajeff, F.; Lindstrom, T. High performing micromachined retroreflector. *Opt. Express* **2003**, *11*, 2459−2473.
(38) Eckhardt, H. D. Simple model of corner reflector phenomena. *Appl. Opt.* **1971**, *10*, 1559−1566.
(39) Bergna, H. E. *The Colloid Chemistry of Silica*; American Chemical Society: Washington, DC (United States), 1994.
(40) Jiang, P.; Ostojic, G. N.; Narat, R.; Mittleman, D. M.; Colvin, V. L. The fabrication and bandgap engineering of photonic multilayers. *Adv. Mater.* **2001**, *13*, 389−393.
(41) Jiang, P.; Bertone, J. F.; Hwang, K. S.; Colvin, V. L. Single-crystal colloidal multilayers of controlled thickness. *Chem. Mater.* **1999**, *11*, 2132−2140.

DOI: 10.1021/acs.langmuir.6b03329
Langmuir 2016, 32, 12869−12875